Dynamical singularities for complex initial conditions and the motion at a real separatrix

Tamar Shnerb and K. G. Kay
Department of Chemistry, Bar-Ilan University, Ramat-Gan 52900, Israel
(Received 31 October 2005; published 10 April 2006)

This work investigates singularities occurring at finite real times in the classical dynamics of one-dimensional double-well systems with complex initial conditions. The objective is to understand the relationship between these singularities and the behavior of the systems for real initial conditions. An analytical treatment establishes that the dynamics of a quartic double well system possesses a doubly infinite sequence of singularities. These are associated with initial conditions that converge to those for the real separatrix as the singularity time becomes infinite. This confluence of singularities is shown to lead to the unstable behavior that characterizes the real motion at the separatrix. Numerical calculations confirm the existence of a large number of singularities converging to the separatrix for this and two additional double-well systems. The approach of singularities to the real axis is of particular interest since such behavior has been related to the formation of chaos in nonintegrable systems. The properties of the singular trajectories which cause this convergence to the separatrix are identified. The hyperbolic fixed point corresponding to the potential energy maximum, responsible for the characteristic motion at a separatrix, also plays a critical role in the formation of the complex singularities by delaying trajectories and then deflecting them into asymptotic regions of space from where they are directly repelled to infinity in a finite time.

DOI: 10.1103/PhysRevE.73.046202 PACS number(s): 05.45.−a, 45.05.+x, 03.65.Sq

I. INTRODUCTION

In this paper we investigate singularities that occur in the classical dynamics of one-dimensional systems at finite real times for complex initial conditions. Our goal is to examine the relationship of such singularities to phenomena observed in ordinary real dynamics. In particular, we explore the connection between such singularities and the unstable behavior that characterizes the purely real motion of double-well systems near separatrices. The results may have implications for the understanding of chaos formation in nonlinear systems.

We refer to the real-time behavior of a classical system with complex initial conditions as complex dynamics (CD). This form of dynamics is directly important for various semiclassical treatments of time evolution. For example, construction of the semiclassical Van Vleck propagator in the ordinary coordinate representation [1,2] requires identification of classical "root" trajectories that travel between two specified positions in a given time. Complex dynamics becomes relevant for classically forbidden processes (e.g., tunneling) since the root trajectories must then have complex initial momenta [3–6]. The time-dependent semiclassical treatment of tunneling [7,8] in the so-called initial value representation [9–11] also requires an analysis of CD, since the integrand in this treatment must be designed to allow deformation of the integration paths to steepest descent contours passing through points that are initial conditions for the same complex root trajectories arising in the Van Vleck approach [7]. Semiclassical propagation in the coherent state representation [12–21] again requires identification of certain root trajectories, but these now involve complex initial conditions for almost all pairs of initial and final states, even for the case of free particle motion [12]. As a result, such a treatment relies on CD even more heavily than the former approaches.

Previous studies of CD in one-dimensional systems have revealed that, for particular choices of initial conditions, the dynamical variables may become infinite at a finite time, even for Hamiltonians that are analytic for real values of the coordinate and momentum [14,15,22]. When one of the initial variables is held fixed, singularities plotted as functions of the real and imaginary parts of the remaining complex initial variable are found to lie along certain continuous 1D curves [14,15] which we call "singularity curves." As the initial conditions vary along such a curve, the time t_* at which the trajectory diverges varies continuously and monotonically. When initial conditions cross such a curve at a point associated with a particular value for t_*, the dynamics for $t > t_*$ changes discontinuously.

Such singularity curves are important for semiclassical theory. In the coherent state representation, the different dynamics obtained upon crossing these curves can yield separate root trajectories that contribute to the semiclassical propagator [14,15]. In the ordinary coordinate representation, determination of root trajectories that describe tunneling may require analytic continuation of the dynamics across the singularity curves which serve as branch cuts [7].

Semiclassical investigations of chaotic tunneling [18,23–26] have focused attention on CD singularities for nonintegrable systems. Such singularities are implicated in the formation of characteristic interference patterns in the scattering probability [18,24–26] and play a role in the determination of the nonlinear resonance interactions associated with tunneling [23].

The singularities of interest here are related to those occurring in real time for the dynamics of complex Hamiltonian systems [27,28] and, especially, to those occurring for complex time in real Hamiltonian systems [29–35]. Singularities of the latter kind arise in semiclassical treatments of time-independent properties for systems undergoing tunneling [29] and time-dependent properties for nonautonomous systems [24–26]. They have also been the subject of great interest due to their relevance for the issue of the integrabil-

ity of classical systems, as implied by the Painlevé-Kowaleskaya conjecture [30–35].

Beyond semiclassical applications and the subject of Painlevé integrability, the present work is motivated by a suspected role of the singularities in the formation of chaos. A connection between complex singularities and real chaotic behavior was established a number of years ago by Greene and Percival [36] for the cases of the standard and semistandard maps. These authors showed that the singularities form "natural boundaries" defining a zone of analyticity about a real torus in complex phase space. For appropriate choices of system parameters, the singularities approach the real axis, the zone shrinks, and global real chaos ensues. Greene and Percival attributed this result to the breakdown of the analyticity requirements [37] for the persistence of KAM tori in perturbed integrable systems. They further conjectured that a similar relationship between the complex singularities and the onset of real chaos should hold for general nonintegrable Hamiltonian systems.

A more common approach to the understanding the formation of chaos relates the onset of this phenomenon to the properties of hyperbolic fixed points (HFPs) and the broken separatrices that emanate from them. Thus, the unstable nature of chaotic motion can be attributed to the instability of the dynamics along the separatrix (e.g., as expressed by the whisker map [38]), the homoclinic entanglement of the stable and unstable manifolds of the HFPs [39,40] and the nature of the separatrix as an accumulation point for nonlinear resonances [38]. The central importance of the separatrix for the chaos that may be formed when an integrable system is perturbed raises the question of how separatrix motion continues in the complex plane. Viewed from the opposite direction, one is led to ask, "What specific form of complex behavior correlates to motion along the separatrix as the initial conditions become real?" Since the real separatrix motion becomes singular at infinite time, one may suspect that it is related to singular trajectories in the complex plane, i.e., that real separatrices are formed by the approach of CD singularities to the real plane. A clarification of this matter might establish a link between the Greene-Percival treatment of chaos formation and the properties of the HFPs.

However, quite apart from the issues described above, a principal factor motivating the present studies is that complex dynamics is a direct generalization of ordinary, real, classical motion. It is, thus, a worthy subject for investigation on fundamental grounds. The singularities that arise in CD are prominent, apparently ubiquitous, phenomena for nonlinear systems. Such divergences affect not only the behavior of singular trajectories but, in certain cases, qualitatively dominate the nature of almost all trajectories of the system (see Sec. III below). It is, therefore, surprising that little systematic work has been directed towards exploring the phenomenology of CD singularities, even for the simplest systems. In particular, the possible relationship of these singularities to unstable, real motion has not received due attention in previous work. Here we take some preliminary steps to remedy this situation by examining the complex dynamics of simple, one-dimensional, systems having potential energy barriers, particularly, double-well systems. The ordinary, real-valued, motion of such systems is characterized by separatrices associated with unstable but (in the absence of nonintegrable perturbations) nonchaotic behavior. For the systems treated, we show analytically and numerically that singular trajectories form the extension of the real separatrix in complex phase space, i.e., that complex singularities accumulate to the real separatrix as the singularity time becomes infinite. Our analysis reveals the role of the hyperbolic fixed point in the formation of the complex singularities and, for particular systems, the relationship between the instability of the singular trajectories and the instability of the real separatrix motion. Questions regarding the degree to which these conclusions remain valid for nonintegrable systems, and the possible mechanistic role of the singularities in the formation of real chaos, are relegated to a separate study.

In Sec. II we present an analytical investigation of the complex singular motion in a quartic double well system, which establishes the relationship of the CD singularities to the real separatrix for this case. In Sec. III we study the complex dynamics of this system numerically to obtain a physical picture of the singular dynamics and to allow comparison with the behavior of more general systems for which analytical treatments are unfeasible. In Sec. IV, we numerically investigate the singular motion of two additional double-well systems, and verify that the behavior is qualitatively similar to that of the quartic case. We, further, identify the properties of the singular trajectories that are responsible for the apparently generality of this behavior for one-dimensional systems having potential barriers. Finally, in Sec. V, we summarize and discuss our findings.

II. ANALYTICAL TREATMENT OF THE QUARTIC DOUBLE WELL

We wish to investigate the dynamics of the double well system defined by the Hamiltonian

$$H = \frac{p^2}{2} + V(q), \tag{1}$$

where the potential energy function is given by

$$V(q) = q^4 - 2q^2. \tag{2}$$

For real values of the coordinate q the potential energy function has minima at $q=\pm 1$, where $V=-1$, and a barrier maximum at $q=0$, where $V=0$. The separatrix for this system thus lies at energy $E=0$.

The equations of motion for this system can be solved analytically. Given the real energy E and real initial position $q_0 \equiv q(0)$, the position at real time t is given by [40]

$$q(t) = q_+ \mathrm{dn}[\sqrt{2} q_+ (t-\tau), k], \tag{3}$$

where dn is the Jacobi elliptic function [41]. In this expression, k is defined as

$$k = (1 - q_-^2/q_+^2)^{1/2} \tag{4}$$

and

$$q_{\pm} = [1 \pm (1+E)^{1/2}]^{1/2} \tag{5}$$

are the turning points for motion at energy E (i.e., the positions where $p=0$). τ is defined by

$$\tau = \frac{1}{\sqrt{2}q_{+}} F(\phi,k) \tag{6}$$

and can be regarded as the time needed for the particle to go from q_0 to q_{+}. Here,

$$\phi = \sin^{-1}\left(\frac{q_{+}^2 - q_0^2}{q_{+}^2 - q_{-}^2}\right)^{1/2} \tag{7}$$

and

$$F(\phi,k) = \int_0^{\phi} \frac{d\alpha}{(1-k^2\sin^2\alpha)^{1/2}} \tag{8}$$

is the elliptic integral of the first kind [41].

These expressions, which describe the ordinary real-valued classical motion of the system, can be analytically continued to complex values of the initial momentum $p=p_x+ip_y$, initial coordinate $q=x+iy$, and time t, in which cases E, k, $q_{\pm}$, τ, and ϕ generally become complex. The singularities in the resulting motion then follow from the known properties of the function dn$u$. Equation (8.147.3) of Ref. [41] can be used to show that

$$q(t) = \sum_{m=-\infty}^{\infty} \sum_{n=0}^{\infty} q_{mn}(t), \tag{9}$$

where

$$q_{mn}(t) = \frac{2q_{+}(-1)^n(2n+1)K'}{[\sqrt{2}q_{+}(t-\tau) - 2mK]^2 + [(2n+1)K']^2}, \tag{10}$$

and where

$$K = \int_0^{\pi/2} \frac{d\alpha}{(1-k^2\sin^2\alpha)^{1/2}} \tag{11}$$

and

$$K' = \int_0^{\pi/2} \frac{d\alpha}{[1-(1-k^2)\sin^2\alpha]^{1/2}} \tag{12}$$

are complete elliptic integrals of the first kind [41]. Equations (9) and (10) show that $q(t)$ has simple poles at times

$$t_{*} \equiv \tau + (2q_{+}^2)^{-1/2}[2mK - (2n+1)iK'] \tag{13}$$

for all positive and negative integers m,n—a result that can also be deduced directly from the known properties of dn [41]. Differentiation of Eqs. (9) and (10) with respect to time further establishes that $p(t)=\dot{q}(t)$ has second-order poles at such singularity times.

The values of $q_{\pm}$, K, and K', depend on E while the value of τ depends both on E and q_0. For real initial conditions, each of these quantities is real and the singularity times t_{*} are complex. Such times are of interest in Painlevé analysis [30–35]. For complex initial conditions, however, the above quantities generally become complex, thus allowing t_{*} to become real. Such real values signify singularities that occur during the real-time evolution of the system and are of direct importance for this work. The complex initial conditions which produce singularities of this kind must satisfy Im $t_{*}=0$ or

$$\mathrm{Im}\{\tau + (2q_{+}^2)^{-1/2}[2mK - (2n+1)iK']\} = 0 \tag{14}$$

for integer (m,n). For each pair (m,n), the solutions of this equation form a three-dimensional surface in the $\mathbb{R}^4$ phase space of initial conditions $(p_0,q_0)=(p_{0x},p_{0y},x_0,y_0)$, where $p_0=p_{0x}+ip_{0y}\equiv p(0)$ and $q_0=x_0+iy_0$ [22]. Thus, if q_0 is fixed, the values of p_0 leading to singularities should form an infinite set of 1D curves in (p_{0x},p_{0y}) space. These are the singularity curves discussed in the Introduction.

We wish to determine the properties of these curves for the special case of real q_0 and complex p_0 with $p_{0x}>0$, $p_{0y}\geqslant 0$, consistent with the conditions chosen for the numerical investigations of Sec. III. It is convenient to express Eqs. (13) and (14) in terms of the combinations of complete elliptic integrals that become real in the limit as $p_{0y}\to 0$ for $p_{0x}>p_s^{+}\equiv[2(2q_0^2-q_0^4)]^{1/2}$, corresponding to Im $E\to 0$ for Re $E>0$. An analysis similar to that of Ref. [42] shows the appropriate combinations to be $K-iK'$ and K'. Thus Eq. (13) becomes

$$t_{*} = \tau + (2q_{+}^2)^{-1/2}[2m(K-iK') + (2j-1)iK'], \tag{15}$$

where $j=m-n$. Defining

$$(2q_{+}^2)^{-1/2}(K-iK') = \rho - i\sigma, \tag{16}$$

$$(2q_{+}^2)^{-1/2}K' = \mu - i\nu, \tag{17}$$

$$\tau = \tau_r + i\tau_i, \tag{18}$$

where ρ, σ, μ, ν, τ_r, and τ_i are real, Eqs. (13) can be expressed as

$$t_{*} = \tau_r + 2m\rho + (2j-1)\nu, \tag{19}$$

while Eq. (14) becomes

$$\tau_i - 2m\sigma + (2j-1)\mu = 0 \tag{20}$$

or, equivalently,

$$\frac{2j-1}{2m} = \frac{2m-2n-1}{2m} = \frac{\sigma}{\mu} - \frac{\tau_i}{2m\mu}. \tag{21}$$

In the Appendix , it is shown that the quantities defined in Eqs. (16)–(18) obey the inequalities $\rho,\sigma,\mu,\nu\geqslant 0$, $1\geqslant\sigma/\mu\geqslant 0$, and $-\sigma\leqslant\tau_i\leqslant\mu$. For $t_{*}>0$, these conditions restrict the values of m and j, for which Eqs. (19) and (21) can be satisfied, to the range $m\geqslant 1$ and $1\leqslant j\leqslant m$ (corresponding to $0\leqslant n\leqslant m-1$). Since σ/μ and τ_i/μ are continuous functions of p_0 in the range considered, Eq. (21) is satisfied by an infinite set of values (j,m) in the neighborhood of any p_0 in the quadrant $p_{0x},p_{0y}>0$. Because this equation determines the positions of the singularity curves, these curves are dense in this region of the complex p_0 plane.

For $p_{0x}>p_s^{+}$, $\sigma/\mu\to 0$ as $p_{0y}\to 0$ (since both $K-iK'$ and K' become real in that limit), while $\sigma/\mu\to 1$ as $p_{0y}\to\infty$ (see

the Appendix). Numerical investigations further verify that σ/μ increases monotonically with p_{0y} for this range of p_{0x}. If the term involving $\tau_i/(2m\mu)$ in Eq. (21) can be neglected, this monotonic behavior allows us to estimate the relative ordering of the singularity curves. Thus, for constant $p_{0x}>p_s^+$, we expect the values of p_{0y} characterizing these curves to decrease as m increases for fixed j and to increase as m increases for fixed n.

For the case $p_{0x}>0$ and $p_{0y}<0$, an analogous treatment can be carried out in terms of the combination of elliptic integrals $K+iK'$ [42] and K'. It can then be shown that the allowed values of m, j, and n for $t_*>0$ are $m\geqslant 1$, $m+1\leqslant j\leqslant 2m$, and $-m\leqslant n\leqslant -1$. For each singularity (m,n) at momentum p_0 in the upper-half plane, there is a corresponding singularity $(m,-n-1)$ at the complex conjugate momentum p_0^* in the lower-half plane.

We now show that all singularity curves converge at $t_*\to\infty$ to the point on the (p_{0x},p_{0y})-plane corresponding to the separatrix $(E=0)$. For small $|E|$, Eq. (5) implies that

$$q_+^2 = 2 + O(E), \tag{22}$$

$$q_-^2 = (-E/2) + O(E^2), \tag{23}$$

while the properties of the complete elliptic integrals imply that [41]

$$K = \ln 8 - (1/2)\ln(-E) + O(E), \tag{24}$$

$$K' = \pi/2 + O(E). \tag{25}$$

Substituting Eqs. (22)–(25) in Eq. (15) and solving for E thus yields

$$E \approx 64e^{-2(t_*-\tau)/m}e^{i\pi(2j-1)/2m}, \tag{26}$$

where, again, $j=m-n$. This result expresses the energy at which the (m,n) singularity occurs as a function of the singularity time t_*, and shows that the singularity condition is asymptotically satisfied for all (m,n) at $E=0$ as $t_*\to\infty$.

If the initial position q_0 is fixed, the values of the initial momentum p_0 corresponding to the separatrix are given by $p_s^\pm=\pm[2(2q_0^2-q_0^4)]^{1/2}$. Choosing $p_0=p_s^\pm+\Delta p$, where Δp is a small complex increment, gives $E\approx p_s^\pm\Delta p$, so that Eq. (26) yields

$$\Delta p \approx (64/p_s^\pm)e^{-2(t_*-\tau)/m}e^{i\pi(2j-1)/2m} \tag{27}$$

for the values of the initial momenta causing singularities. This establishes that, as $t_*\to\infty$, all singularity curves (plotted as p_{0y} vs p_{0x}) converge to the points $p_s^\pm$, which are on the real axis for real values of q_0 in the range $-\sqrt{2}\leqslant q_0\leqslant\sqrt{2}$. Since $\mathrm{Im}\,\tau\to 0$ as $\mathrm{Im}\,E\to 0$, the curves approach $p_s^\pm$ at $2m$ distinct angles

$$\theta_{jm} = \pi\left(\frac{2j-1}{2m}\right) \tag{28}$$

for each m, where j takes on values $1,2,\ldots,2m$.

We note that an entirely similar treatment can be applied to analyze singularity curves in the space of complex initial positions. Thus, if the initial momentum is held fixed at a real value in the range $-\sqrt{2}\leqslant p_0\leqslant\sqrt{2}$, Eq. (26) shows that the coordinate values associated with singularities obey

$$\Delta q \approx [64/V'(q_s)]e^{-2(t_*-\tau)/m}e^{i\pi(2j-1)/2m}, \tag{29}$$

where $\Delta q=q_0-q_s$, q_s is one of the four real values for q corresponding to the separatrix $[p_0^2/2+V(q_s)=0]$, and $V'=dV/dq$. This establishes that all singularity curves, plotted as y_0 vs x_0, approach one of the separatrix positions q_s on the x_0 axis as $t_*\to\infty$.

We wish to establish the relationship between the limiting CD singularities, obtained as $t_*\to\infty$, and the ordinary real dynamics of the system at the separatrix. To investigate this issue, we write Eq. (9) as

$$q(t) = \sum_{m-\infty}^{\infty} q_m(t), \tag{30}$$

where

$$q_m(t) \equiv \sum_{n=0}^{\infty} q_{mn}(t). \tag{31}$$

Using the identity

$$\mathrm{sech}\, z = 2\pi\sum_{k=0}^{\infty}\frac{(-1)^k(k+1/2)}{z^2+[(k+1/2)\pi]^2} \tag{32}$$

(which can be obtained from the partial fraction expression for $\csc z$ [43]) and Eq. (10), we obtain

$$q_m(t) = \frac{\pi q_+}{2K'}\,\mathrm{sech}\left(\frac{\pi}{2K'}[\sqrt{2}q_+(t-\tau)-2mK]\right). \tag{33}$$

Applying Eqs. (22)–(25) for small E now yields the simple result

$$q_m(t) \approx 2q_+\frac{(-EW_{mt})^m}{E^{2m}+W_{mt}^{2m}}, \tag{34}$$

where

$$W_{mt} \equiv 64e^{-2(t-\tau)/m}. \tag{35}$$

This shows that q_m has $2m$ distinct poles at complex energies $E=W_{mt}e^{i\pi(2j-1)/2m}$, $j=1,2,\ldots,2m$, in agreement with Eq. (26). These are the only singularities in q_m.

This result establishes that, for fixed t, $q(t)$ is an analytic function of E for all real E. Furthermore, although all singularities of $q(t)$ converge to $E=0$ as $t\to\infty$ $(W_{mt}\to 0)$, $q(t)$ remains an analytic function of energy at $E=0$ in that limit. One way of viewing this is to write Eq. (34) as

$$q_m(t) \approx 2\pi(-1)^m q_+ E^m \Delta(E^m), \tag{36}$$

where $\Delta(E^m)\equiv\pi^{-1}W_{mt}^m/(E^{2m}+W_{mt}^{2m})$. As $W_{mt}\to 0$, $\Delta(E^m)$ approaches the Dirac delta function $\delta(E^m)$ so that $\Delta(E^m)$ vanishes for all $E\neq 0$. The remaining singularity at $E=0$ is removed by the factor E^m which causes $\lim_{t\to\infty}q_m(t)=0$ for all E [consistent with the property $x\delta(x)=0$].

Despite this cancellation of divergence, the CD singularities lead to a certain residual form of singular behavior for the real separatrix motion. This is suggested by the rapid

variation of q_m as a function of real E near $E=0$ for small W_{mt}. This variation is due to the opposing effects of two factors in Eq. (36): E^m, which vanishes at $E=0$, and Δ, which becomes large near $E=0$ for small W_{mt}, reflecting the confluence of the $2m$ CD singularities to the separatrix. As a result, $|q_m|$ varies as a function of energy between the extreme values of 0 for $E=0$ and q_+ for $E=\pm W_{mt}$, and these changes occur over a decreasingly small energy range as $W_{mt}\to 0$.

To explore this matter in more detail, we examine the derivative

$$\frac{\partial q_m(t)}{\partial E} = 2mq_+ W_{mt} \frac{(-EW_{mt})^{m-1}(E^{2m} - W_{mt}^{2m})}{(E^{2m} + W_{mt}^{2m})^2} \tag{37}$$

for $m \geqslant 1$. Although, for fixed t, this function is analytic on the real E axis, singular behavior emerges when we let $W_{mt}=\alpha E$ where α is a real constant. This is equivalent to choosing the time t such that the particle is in the vicinity of one of the outer turning points $\pm q_+$ (i.e., not too near $q=0$), regardless of the energy. Then we find that

$$\frac{\partial q_m(t)}{\partial E} = \frac{1}{E} \frac{mq_+(-\alpha)^m(\alpha^{2m} - 1)}{(\alpha^{2m} + 1)^2}, \tag{38}$$

which has a pole at $E\to 0$ for $|\alpha| \neq 1$. Since only a single term effectively contributes to Eq. (30) for $q(t)$ in this limit, the above pole also dominates $\partial q(t)/\partial E$.

The singularity appearing in Eq. (38) reflects the instability of the real motion at the separatrix, associated with the sudden change in the long-time behavior of the trajectory as the energy passes through 0. Although the mathematical nature of this singularity is different than that of the CD singularities, it originates from the confluence of the CD singularities at the separatrix at infinite time. It is a residual form of singular CD behavior that survives after the divergence is removed. This establishes the relationship between the complex singularities and the real dynamics at the separatrix for the present system.

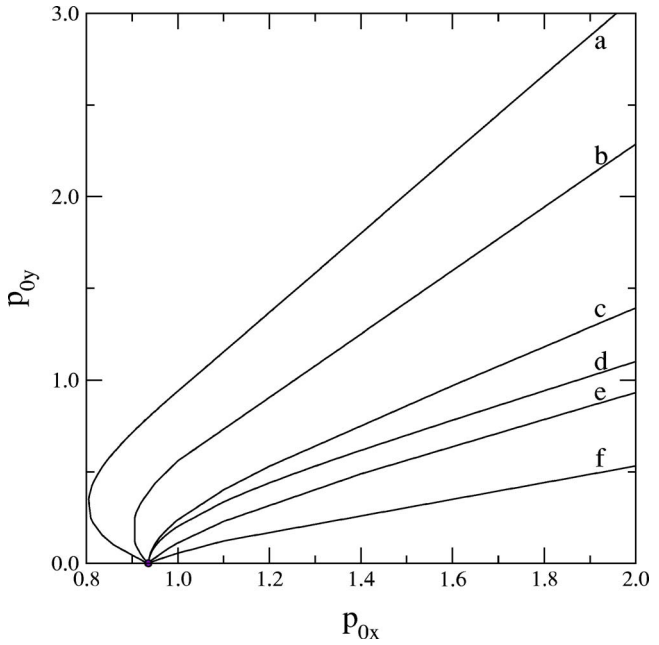

FIG. 1. Some singularity curves for the quartic double-well system. The point marked by a dot on the real axis corresponds to the separatrix momentum p_s^+.

III. NUMERICAL TREATMENT OF THE QUARTIC DOUBLE WELL

In this section we describe numerical calculations that allow us to examine the CD singularities for the above system and to investigate the trajectories associated with these phenomena. The objective is to clarify the physical origin of the analytical results and to express the singular behavior in a form that allows comparison to results for other systems, where analytical results are not available.

Figure 1 shows a few singularity curves obtained by numerically integrating Hamilton's equations of motion for this system. The curves describe complex values of the initial momentum (p_{0x}, p_{0y}) that yield singularities for the fixed, real, initial value $q_0=0.5$ of the coordinate, describing the particle in the right well at $t=0$. Only curves in the quadrant $p_{0x}>0$, $p_{0y}>0$ are displayed here but a mirror image of this

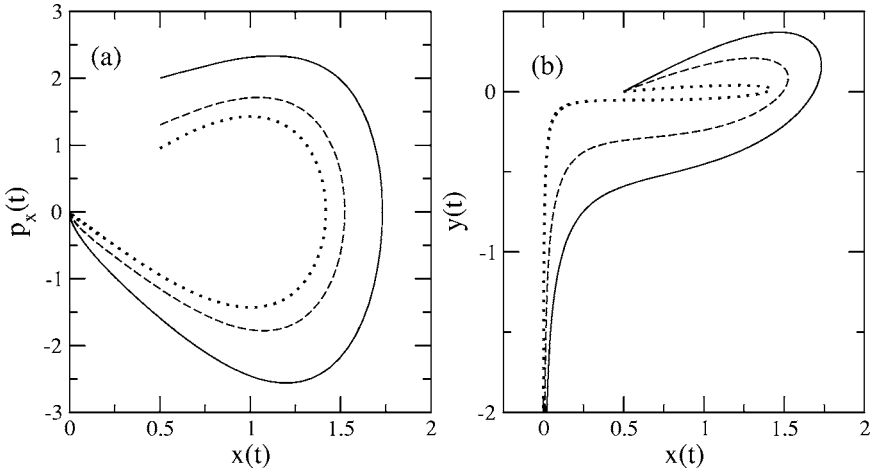

FIG. 2. Singular trajectories projected on the (x,p_x) plane [subfigure (a)] and the (x,y) plane [subfigure (b)] for three different points along curve d in Fig. 1. The values of (p_{0x},p_{0y}) for the three trajectories shown are solid curve: (2.00,1.101), dashed curve: (1.30,0.531), dotted curve: (0.950,0.0920).

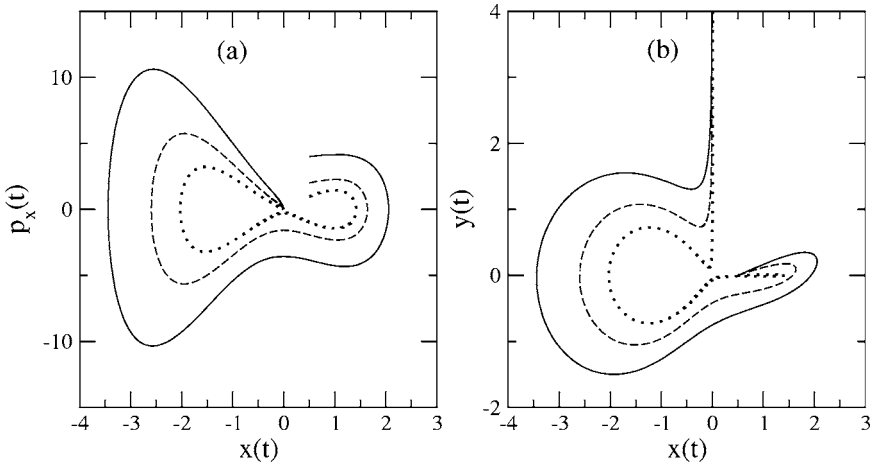

FIG. 3. Singular trajectories projected on the (x,p_x) plane [subfigure (a)] and the (x,y) plane [subfigure (b)] for three different points along curve f in Fig. 1. The values of (p_{0x},p_{0y}) for the three trajectories shown are solid curve: (4.00,1.364), dashed curve: (2.00,0.531), dotted curve: (0.970,0.0314).

set exists for $p_{0y}<0$. Additional sets of curves also appear for $p_{0x}<0$. However, since $q_0\neq 0$ in the present calculations, these are only similar to, but not precisely, mirror images of the curves for $p_{0x}>0$.

To generate these results, Hamilton's equations of motion, together with the differential equations for the monodromy elements $\partial p(t)/\partial p_0$ and $\partial q(t)/\partial p_0$, were integrated using a fixed time-step Runge-Kutta algorithm. Singularities were assumed to occur when $|\partial p(t)/\partial p_0|$ attained a large value [although we could have used large values for $|p(t)|$ or $|q(t)|$ as singularity criteria]. The search for singularity curves was carried out by examining the dynamics for finely spaced intervals along p_{0y} and specified values of p_{0x} [22].

The results shown in Fig. 1 are qualitatively consistent with the conclusions of Sec. II. Although only six singularity curves are displayed, many more are actually observed. As discussed below, such curves indeed seem to form an infinite sequence, as suggested by the analytical results. All curves appear to converge to the point $p_s^+=[2(2q_0^2-q_0^4)]^{1/2}\approx 0.9354$ on the real axis, corresponding to the momentum at the separatrix. Along a given curve, the time t_* at which the singularity occurs is found to increase as p_{0y} decreases, consistent with $t_*\to\infty$ as $p_0\to p_s^+$, as suggested by Eq. (27). In addition, the various curves are seen to approach p_s^+ at specific angles [also see Fig. 6 below], suggesting that each curve is associated with a particular pair of integers (m,n) or (m,j), consistent with Eq. (28).

The physical meaning of these results can be made clearer by examining the singular trajectories associated with the various curves. A few such trajectories are projected on the (x,p_x) and (x,y) planes in Figs. 2–4. The divergence of the trajectories is more directly evident in plots of y vs x than in those of p_x vs x since $y(t)\to\pm\infty$, but $x(t)\to 0$ and $p_x(t)\to 0$ at the singularities.

The plots of $p_x(t)$ vs. $x(t)$ are reminiscent of the well-known phase portraits for the real motion of the system [40]. However, whereas the real trajectories either remain in a specific potential well for all time $(E<0)$ or alternate between the two wells for all time $(E>0)$, the present complex trajectories generally have an intermediate nature. They remain in a particular well for a certain number of cycles and then move to the other well. Thus, a CD trajectory can be characterized by its sequence of the cycles in the two wells. This allows one to conveniently represent a singular trajectory by a finite code of the form $r^{k_1}l^{k_2}r^{k_3}\cdots$ where, e.g., r^{k_1} denotes k_1 cycles in the right well and l^{k_2} represents k_2 cycles in the left well. Figures 2–4 show that all trajectories associated with a particular singularity curve have the same code while trajectories associated with different singularity curves have different codes. For example, the codes for the trajectories plotted in Figs. 2–4, associated with curves d, f, and c in Fig. 1, are r,rl, and r^2l, respectively. Table I presents the codes for the remaining curves in Fig. 1.

A detailed examination of the arrangement of the singularity curves in the (p_{0x},p_{0y}) plane reveals the following pat-

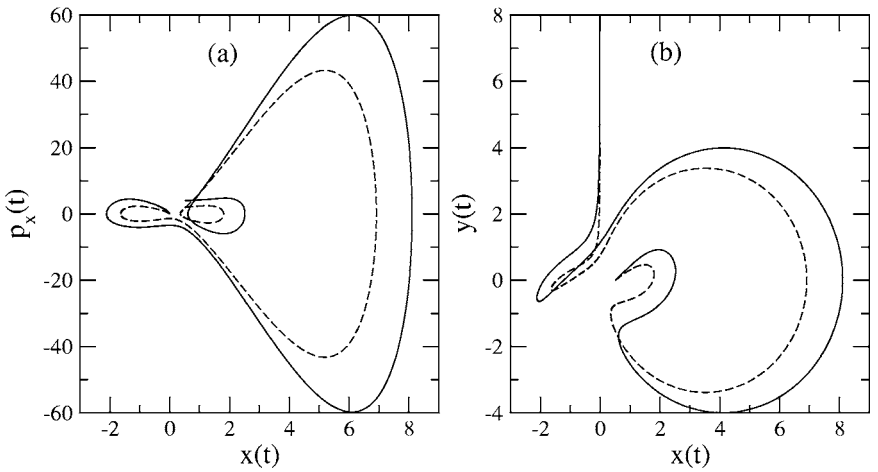

FIG. 4. Singular trajectories projected on the (x,p_x) plane [subfigure (a)] and the (x,y) plane [subfigure (b)] for two different points along curve c in Fig. 1. The values of (p_{0x},p_{0y}) for the trajectories shown are solid curve: (4.00,3.552), dashed curve: (2.00,1.393).

TABLE I. The codes, values of integers m and n, and angles θ_{jm} for the singularity curves presented in Fig. 1.

Curve	Code	m	n	θ_{jm}
a	r^2	2	0	$3\pi/4$
b	r^2l^2	4	1	$5\pi/8$
c	r^2l	3	1	$\pi/2$
d	r	1	0	$\pi/2$
e	rl^2r	4	2	$3\pi/8$
f	rl	2	1	$\pi/4$

tern. For fixed $p_{0x}>p_s^+$, curves belonging to the sequence r^k, $k=1,2,\ldots$, are located at values of p_{0y} that increase with k. Beneath curve r^{k_1} (and above r^{k_1-1} for $k_1>1$) are curves $r^{k_1}l^{k_2}$ at values of p_{0y} that increase with k_2. Beneath $r^{k_1}l^{k_2}$ (and above $r^{k_1}l^{k_2-1}$ for $k_2>1$) are curves $r^{k_1}l^{k_2}r^{k_3}$at values of p_{0y} that increase with k_3. This pattern appears to repeat on ever finer scales *ad infinitum*. Although singularity curves consistent with all values of $k_1,k_2,\ldots$, do not exist (see below), the curves seem to form a dense set, so that every nonsingular trajectory can be made singular by an infinitesimal adjustment of the initial conditions. The sequence of singularity curves with codes $rl,rlrl,rlrlrl,\ldots\equiv(rl)^k$ converges to the real axis at $p_{0x}>p_s^+$ as $k\to\infty$, consistent with untrapped real trajectories with energies $E>0$, while the sequence of curves with codes r, r^2, $r^3,\ldots\equiv r^k$ converges to the real axis at $p<p_s^+$ as $k\to\infty$, consistent with real trajectories with $E<0$ that are trapped in the right well.

The relation between this code and the integers m and n introduced in Sec. II can be understood by expressing the singularity time as

$$t_* = \int_{\mathcal{C}} dq/p(q,E) = \int_{\mathcal{C}} [2(E-q^4+2q^2)]^{-1/2}dq, \quad (39)$$

where the integration contour $\mathcal{C}$ coincides with the complex singular trajectory in q space, extending from initial position q_0 to $q(t_*)=\pm i\infty$. As illustrated in Fig. 5, such a trajectory generally winds around the four turning points $\pm q_\pm$ a number of times in (x,y) space before becoming divergent. For the initial conditions investigated here, the first turning point is always q_+ and the final turning point prior to divergence is always $\pm q_-$. Such turning points are square-root branch cuts in Eq. (39) and are the only singularities in the integrand. Thus, $\mathcal{C}$ can be deformed to run between the q_0 and q_+, between various pairs of turning points, and between the final turning point and $\mp i\infty$. As a result, the integral, representing the real time t_*, can be broken down into a sum of individually complex contributions: a time for passage from q_0 toq_+ (denoted by τ), complex times for passage between specific pairs of turning points, and a time for passage between the last turning point and $\mp i\infty$. However, examination of Eqs. (11) and (12) shows that, apart from τ, each of these times can be expressed in terms of the complete elliptic integrals K and iK'. For example, the times for direct passage between q_+ and q_-, between q_+ and $-q_+$, and between $\pm q_-$ and $\mp i\infty$ are, respectively, cK, $2c(K-iK')$, and $c(K-iK')$, where $c=(2q_+^2)^{-1/2}$. This allows one to express t_*in a form similar to that of Eq. (13) and leads to an identification of m and n in terms of the code for singular trajectory (see the caption of Fig. 5 for an example). The outcome of this analysis is that $m=k_1+k_2+\cdots+k_{n+1}$ is the length of the code and n is the number of transitions in the code from r to l and l to r.

This identification allows us to relate the observed hierarchy of singularity curves to the discussion of Sec. II. Thus, for example, the increasing values of p_{0y} for the sequence of singularities $r,r^2,r^3,\ldots$, corresponding to $(m,n)=(1,0),(2,0),(3,0),\ldots$, is consistent with the expectation that p_{0y} should increase as m increases for constant n. The decreasing values in p_{0y} for the sequence of singularities $r,rl,rlr,\ldots$, with $(m,j)=(1,1),(2,1),(3,1),\ldots$, is consistent with the expectation that p_{0y} should decrease as m increases for constant j. Note, however, that certain details of the hierarchy can be explained only by taking into account additional considerations. For example, the choice $(m,n)=(3,1)$

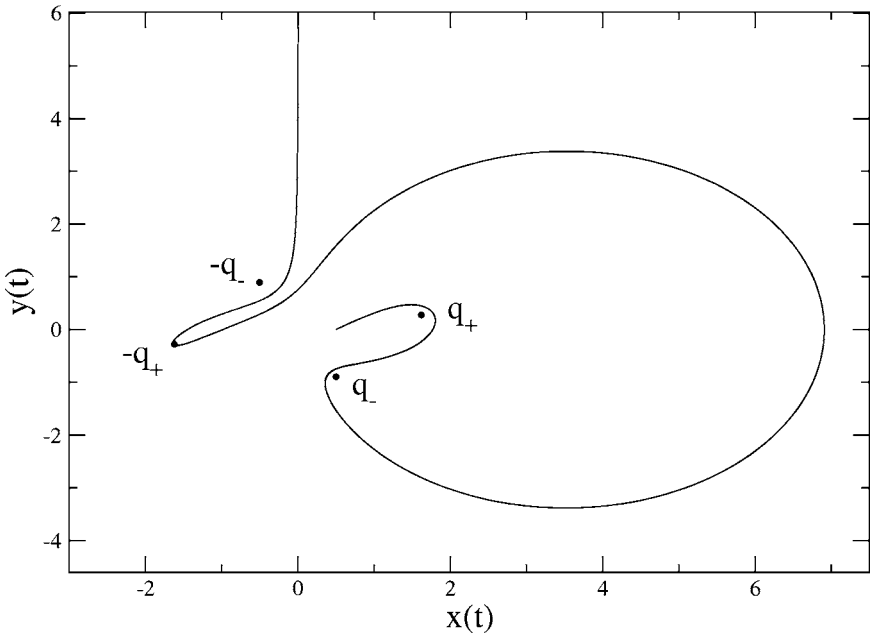

FIG. 5. Singular trajectory of type r^2l and turning points. Considered as an integration path, this trajectory can be deformed into a segment from the initial position to q_+, followed by segments that pass through $q_-,q_+,-q_+,-q_-$, and $i\infty$ in succession. The complex passage times for these segments are $\tau,cK,cK,2c(K-iK'),cK$, and $c(K-iK')$, respectively, where $c=(2q_+^2)^{-1/2}$. Thus, the singularity time t_* in this case is $\tau+c(6K-3iK')$, consistent with $m=3,n=1$ in Eq. (13).

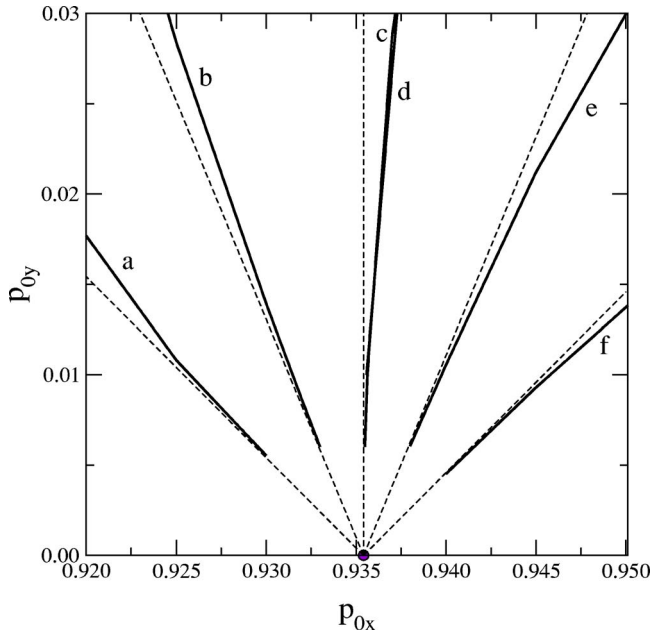

FIG. 6. (Color online) Magnified portion of Fig. 1 near $p=p_s^+$. The dashed lines are rays from p_s^+ at the angles θ_{jm} given in Table I.

corresponds to two possible codes rl^2 and r^2l but can yield only one singularity curve. The issue of which curve actually appears is determined by its position relative to the curve r. The key role of this position can be understood by recalling that the complex motion must vary continuously with the initial conditions for times prior to singularities. The location of the sequence $rl, rlr, rlrl, \ldots$, below r implies that all trajectories lying below r (the earliest singularity) must begin with the code $rl, \ldots$, and similar considerations imply that all trajectories between r and r^2 must begin with the code $r^2l, \ldots$. However, although the discussion following Eq. (21) suggests that the $(3,1)$ curve [for which $(2j-1)/2m=1/2$] should lie between curves rl and r^2, it does not establish whether it lies below or above curve r [for which $(2j-1)/2m=1/2$ also]. This determination requires knowledge of the numerical values of τ_i/μ that are neglected in the above estimates. In practice, these values place the $(3,1)$ curve above r so that the singularity curve actually observed is r^2l,while the curve rl^2 does not exist. We mention that the nonunique correspondence of (m,n) to a particular code is the rule rather the exception. Thus, the determination of which hierarchy members are observed and which are absent usually requires considerations similar to those above.

The assignment of integers (m,n) to the r-l codes also make it possible to apply Eq. (28) to determine the values of θ_{jm} that correspond to the various computed singularity curves. These assignments imply that θ_{jm} should be 0 for curve $(rl)^\infty$ and π for curve r^∞. Table I presents the values of m, n, and the predicted θ_{jm} for the curves appearing in Fig. 1. Figure 6 verifies that these values for θ_{jm} agree with the observed angles for approach of the curves to p_s^+.

The plots of the trajectory dynamics allow us to identify the asymptotic mechanism for the singular behavior. Panels (b) of Figs. 2–4 show that the divergences for the present system always occur along a portion of the trajectory characterized by $y(t)\to\pm\infty$ and $x(t)\to 0$. This behavior is easily understood by examining the force $F=-\partial V(q)/\partial q=F_x+iF_y$ that acts on the particle as $|q|\to\infty$. For double-well systems, divergence will occur if the force along a particular curve in q space repels the particle outwards and is sufficiently strong to cause the particle to reach infinity in a finite time. We call a curve along which these conditions are asymptotically obeyed a divergence channel. More specifically, the conditions that should be satisfied as $|q|\to\infty$ are

$$|F| \sim O(|q|^a), \quad a>1 \tag{40}$$

(which implies that the force is sufficiently strong [44]),

$$F_y/F_x \sim y/x \tag{41}$$

(which implies that F is directed along the channel), and

$$xF_x + yF_y > 0 \tag{42}$$

(which implies that the force along the channel is repulsive).

For the present system one easily finds

$$F_x = 4x(1+3y^2-x^2) \tag{43}$$

and

$$F_y = 4y(1-3x^2+y^2). \tag{44}$$

Condition (40) is clearly obeyed in all directions of space for large $|q|$, however, conditions (41) and (42) are asymptotically obeyed only for $|y|\to\infty$ and $x\to 0$. Thus, the divergence channel lies along the positive or negative y axis.

For large $|q|$ in the vicinity of these channels, the force components behave as

$$F_x \sim 12xy^2, \quad F_y \sim 4y^3 \tag{45}$$

and the asymptotic singular motion can be determined by solving Newton's equations $\ddot{x}=F_x$, $\ddot{y}=F_y$. If the "initial conditions" at time t_1 are defined to be $x=x_1, y=y_1$, where $|y_1/x_1| \gg 1$ and $x_1y_1^3=O(1)$, the trajectory for times $t_* > t \geqslant t_1$ is found to be

$$x(t) = x_1[1-\sqrt{2}|y_1|(t-t_1)]^3,$$

$$y(t) = \frac{y_1}{1-\sqrt{2}|y_1|(t-t_1)}, \tag{46}$$

and the singularity time is seen to be $t_*=t_1+1/(\sqrt{2}|y_1|)$. This result is consistent with the divergent behavior of the motion observed in the numerical calculations.

To understand the nature of the trajectories described by Eqs. (46), we may substitute these equations and their time derivatives in Eq. (1) and examine the resulting expression for the Hamiltonian. Such a treatment immediately reveals that the condition $H=E$ is satisfied asymptotically only if x_1 and y_1 are chosen to obey $2x_1y_1^3=\mathrm{Im}\,E$. This shows that the above expressions for $x(t)$ and $y(t)$ are valid only for a very specific choice of initial conditions, asymptotically equivalent to those implied by Eq. (14). Any deviation from these conditions causes the trajectory to veer asymptotically to the right or left of the y axis so that it falls off the divergence

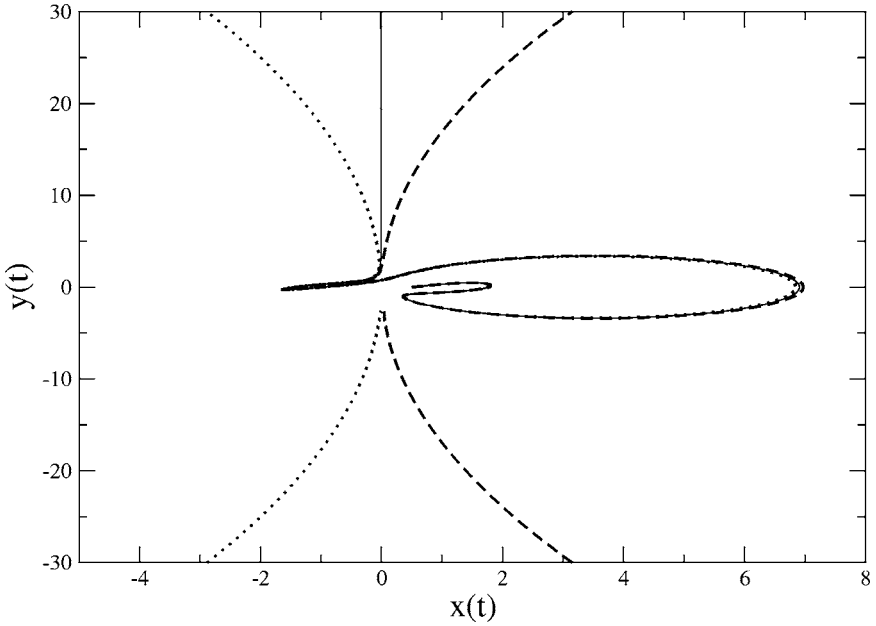

FIG. 7. Singular trajectory of type r^2l obtained with $(p_{0x},p_{0y})=(2.00,1.393)$ (solid curve) and portions of apparently nonsingular trajectories obtained with $(p_{0x},p_{0y})=(2.00,1.390)$ (dashed curve) and $(p_{0x},p_{0y})=(2.00,1.396)$ (dotted curve). In the latter two cases, the trajectories go off scale at the top of the graph and return on the bottom after forming a partial loop on the right or left. Although these trajectories are terminated at $t=5.60$ to avoid complicating the figure, they actually continue without diverging for very long times.

channel, causing the motion to become nonsingular.

Consistent with the analysis of Sec. II, these considerations imply that motion along the divergence channels is unstable. The instability of the singular trajectories is clearly observed in numerical calculations using the full Hamiltonian of Eq. (1). As illustrated in Fig. 7, a minute change of initial conditions from those corresponding to a singularity curve transforms the divergent portion of a singular trajectory into an additional cycle in one of the wells, followed by further nonsingular motion. The identity of this well is different for initial conditions above and below the singularity curve. Thus, the r^2l singular trajectory becomes a nonsingular trajectory of type $r^2lr,\ldots$, for p_{0y} below the singularity curve and a nonsingular trajectory of type $r^2l^2,\ldots$, for p_{0y} above the singularity curve. This behavior is consistent with previous observations [7,14,15] of sudden changes in the nature of generic nonsingular trajectories as the initial conditions cross a singularity curve. From the present perspective, it is interesting to note the qualitative similarity between this phenomenon, which occurs at finite times for complex energies, and the abrupt change in the behavior of trajectories which occurs at infinite times at the real separatrix energy.

Although the singular trajectories occupy a zero measure in the phase space of initial conditions, their density implies that they qualitatively dominate the dynamics of typical nonsingular trajectories. As illustrated in Fig. 8, such nonsingular trajectories are unbounded, with dynamical variables that can become arbitrarily large at an infinite number of times. These correspond to values of t_* for the infinite number of singularities with initial conditions that are arbitrarily close to those of the nonsingular trajectory. Thus, the importance of the singularities is not limited to the singular trajectories; they have a very strong qualitative influence on the nature of the generic trajectories of this system.

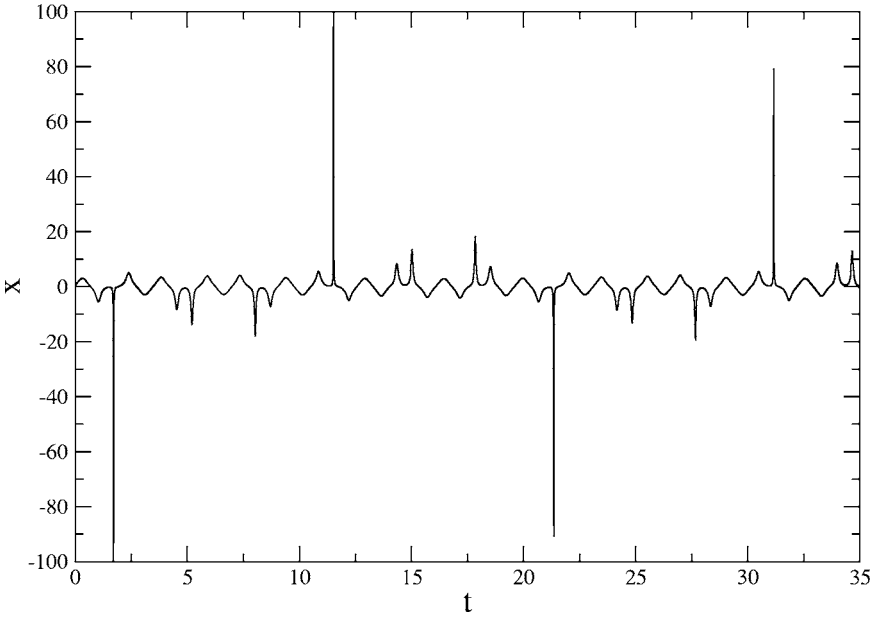

FIG. 8. Real part of the coordinate vs time for a nonsingular trajectory with $q_0=(0.5,0.0)$ and $p_0=(10.0,4.000)$. The large values of $|x|$ are associated with singularities for nearby initial conditions, e.g., the rl singularity which occurs at $t_*=1.71$ for $p_{0y}=3.920$, and the $rl^2rlrl^2rlrl^2rlr$ singularity which occurs at $t_*=11.53$ for $p_{0y}=3.987$ (with the same values of q_0 and p_{0x} in all cases).

Examination of (x,y) plots of singular trajectories, such as those in Figs. 2–4, as well as many others, reveals an interesting, consistently observed feature: entrance to a divergence channel is always found to be immediately preceded by deflection of the trajectory from the region near the origin [45]. This deflection becomes increasingly sharp as the initial conditions approach those of the separatrix. The feature of the potential energy function $V(q)$ responsible for this behavior is the saddle at $(x,y)=(0,0)$ which creates a hyperbolic fixed point (HFP) for both the real and complex dynamics of this system. In fact, linearizing Newton's equation near such a point yields $\ddot{x}=4x$ and $\ddot{y}=4y$, which shows that the resulting complex dynamics is completely analogous to that of a real two-dimensional system with potential energy function $U(x,y)=-2(x^2+y^2)$, describing a barrier at $x=y=0$. Thus, the trajectory asymptotically approaches and leaves the region about the barrier maximum along straight lines in (x,y) space emanating from that point, allowing the asymptotic motion to be characterized by approach and deflection angles. Furthermore, as the energy tends to that of the barrier $(E=0)$, the time that the particle remains near the HFP diverges logarithmically (see below). In that limit, the deflection angle of the particle becomes infinitely sensitive to the initial conditions so that arbitrarily small changes in these conditions cause the deflection direction to take on any value.

IV. NUMERICAL TREATMENT OF ADDITIONAL SYSTEMS

For the quartic double-well system, we have shown both analytically and numerically that the real separatrix is the asymptote of the complex singularities as $t_* \to \infty$. Furthermore, we have obtained some numerical results suggesting that the HFP, responsible for the characteristic behavior of the system at the real separatrix, may also play a mechanistic role in the formation of CD singularities. In this section we explore whether such behavior occurs for more general cases by numerically investigating two additional one-dimensional double-well systems. The different asymptotic forms of the potentials as $q \to \infty$ cause the singular dynamics of these systems to be very different from each other and from that of the first system. Nevertheless, the results for the new systems again indicate that the HFP plays a critical role in the singularity dynamics. By analyzing the common features of the singular trajectories for the present three systems as well as for other systems that we have studied, we are led to identify those properties that cause CD singularities to approach the separatrix for a class of one-dimensional systems having potential barriers.

A. Second system

We turn our attention to the double-well system defined by the Hamiltonian of Eq. (1) with the potential

$$V(q) = \cosh q - q^2. \tag{47}$$

This function rises more steeply than that of the quartic system for large real values of q. It is easily established that the components of the force for the present system are given by

$$F_x = 2x - \sinh x \cos y, \tag{48}$$

$$F_y = 2y - \cosh x \sin y. \tag{49}$$

Substituting these expressions in Eqs. (40)–(42) for the case $|q| \to \infty$ yields the conditions

$$|x| \to \infty, \quad y \to (2k+1)\pi \tag{50}$$

for the divergence channels, where k is any integer. We note that the number and nature of these channels are very different than for the quartic system: instead of only two channels, coinciding with the positive and negative y axis, the present system has an infinite number of channels, each asymptotically parallel to the x axis.

Although we have not investigated the pattern of singularity curves for the present system in great detail, their arrangement in (p_{0x},p_{0y}) space seems to be more complicated than that observed for the quartic system, consistent with a separate set of curves for each of the infinite number of channels. Figure 9 shows two such curves obtained with the real initial value for the coordinate $q_0=0.1$. It is seen that both curves asymptotically approach the value $p_s^+ \approx 0.10$ corresponding to the separatrix $(E=1)$ for this case. Examination of the singularity times indicates that, as for the first system, they increase along the curve as it approaches p_s^+.

Figure 10 reveals that the lower singularity curve of Fig. 9 describes singular trajectories of type *rl* that diverge in channel $k=0$ of Eq. (50) (corresponding to $x \to \infty$, $y \to \pi$) while the upper curve describes singular trajectories of type *r* that diverge in channel $k=-2$ (corresponding to $x \to -\infty$, $y \to -3\pi$). Interestingly, despite the differences between the divergence channels for the present and quartic double well systems, entrance to a divergence channel is, still, always immediately preceded by a critical deflection from the HFP at $q=0$.

B. Third system

Finally, we consider the double-well system with Hamiltonian given by Eq. (1) and potential energy function

$$V(q) = e^{\alpha q^2} - \beta q^2, \ \alpha,\beta > 0 \tag{51}$$

which, for large real values of q, increases even more rapidly than the potential of Eq. (47). The components of the force in this case are

$$F_x = -2\alpha e^{\alpha(x^2-y^2)}[x\cos(2\alpha xy) - y\sin(2\alpha xy)] + 2\beta x, \tag{52}$$

$$F_y = -2\alpha e^{\alpha(x^2-y^2)}[y\cos(2\alpha xy) + x\sin(2\alpha xy)] + 2\beta y, \tag{53}$$

and application of Eqs. (40)–(42) shows that divergence channels for the present system are described by

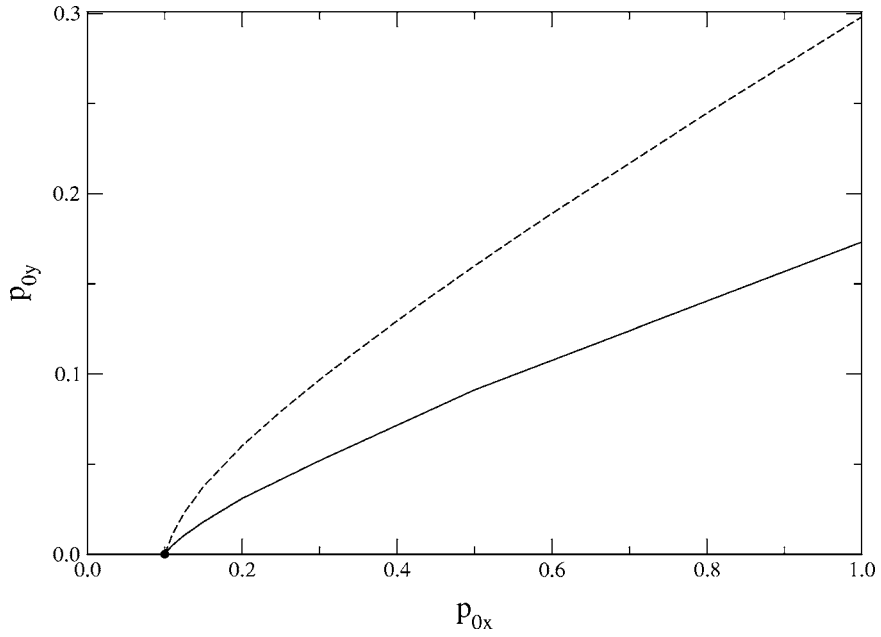

FIG. 9. Two singularity curves for the second system. The dot marks the separatrix momentum p_s^+.

$$|x| \to \infty,\ 2\alpha xy \to (2k+1)\pi, \tag{54}$$

where k is any integer. These channels correspond to hyperbolic branches in the xy plane and are very different from those for the two previous systems.

Figure 11 shows two singularity curves for this system, obtained for parameters $\alpha=0.2$, $\beta=2.0$, and with initial coordinate $q_0=1.2$. As in the previous cases, the curves appear to asymptotically approach the separatrix momentum which is calculated to be $p_s^+ \approx 2.257$. Figure 12 displays trajectories associated with these curves and shows that the lower and upper singularity curves describe trajectories of types rl and r, respectively. This figure also suggests that both trajectories diverge into channels corresponding to $k=0$ in Eq. (54). As for the previous systems, the trajectories are found to be deflected by the HFP immediately (less than half a cycle of motion) before entering a divergence channel, again suggesting that such deflections are involved in the mechanism of singularity formation.

C. Approach of CD singularities to the separatrix for more general systems

For each of the three systems examined here, the singularity curves are observed to approach the separatrix as the singularity time becomes infinite. Although not reported in this paper, we also have observed similar behavior in a number of other one-dimensional systems having potential energy barriers, including those with nonconfining potentials, such as the Eckart system $[V(q)=\mathrm{sech}^2 q]$, and those with multiple barriers, such as the pendulum $[V(q)=-\cos q]$. In-

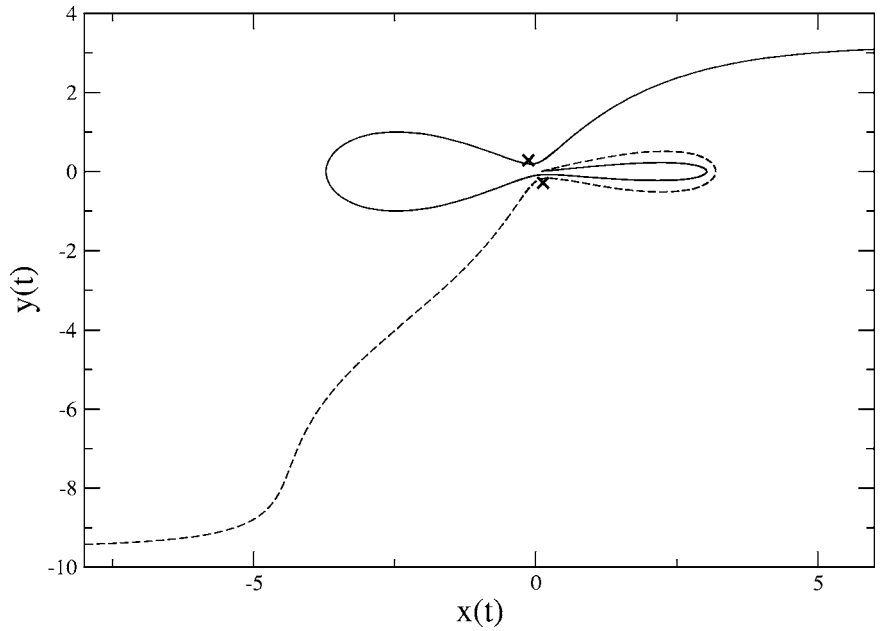

FIG. 10. Singular trajectories taken from the singularity curves in Fig. 9. The solid curve is obtained for $p_0=(0.3,0.05385)$, corresponding to a point on the lower singularity curve, and the dashed curve is obtained for $p_0=(0.3,0.1234)$, corresponding to a point on the upper singularity curve. The $\times$'s mark turning points $\pm q_-$ for the dashed curve. On the scale shown, they are practically identical to the $\pm q_-$ for the solid curve.

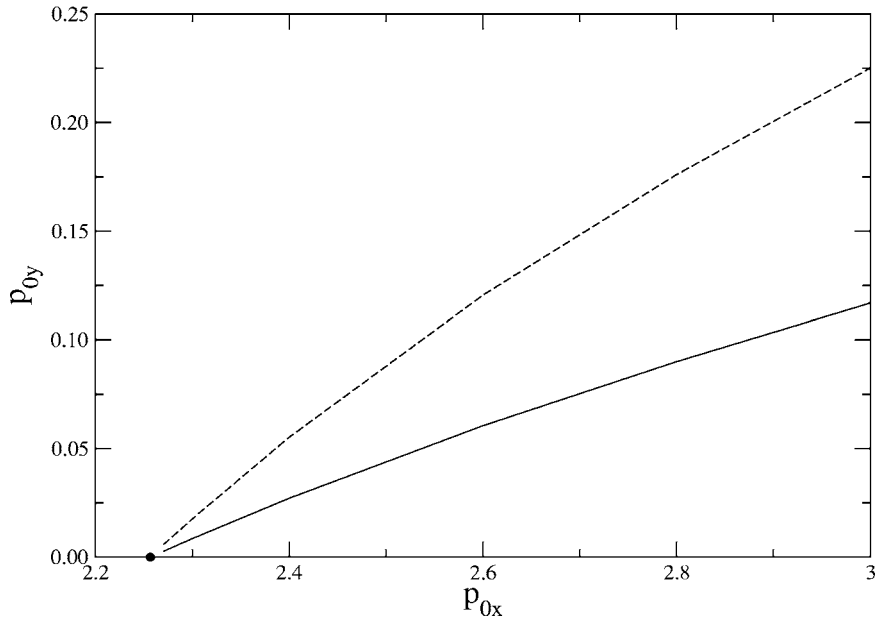

FIG. 11. Two singularity curves for the third system. The dot marks to separatrix momentum p_s^+.

deed, for these two specific examples, such behavior can be proven analytically. The cases studied suggest that the approach of the CD singulatities to the separatrix may be a general feature for one-dimensional systems with potential barriers. In this subsection we attempt to explain the common occurrence of this behavior by identifying the underlying properties of the singular trajectories. This analysis leads to a clearer understanding of the role of the HFP in the singularity dynamics.

For simplicity, let us consider an arbitrary one-dimensional potential $V(q)$ with a single maximum at $q=q_s$, and let us define $E_s \equiv V(q_s)$. Generalization to multiple maxima is straightforward. If we denote by $\mathcal{C}$ the curve in complex q space formed by a singular trajectory, the singularity time can be expressed as $t_*=\int_{\mathcal{C}} dq/p(q,E)$, as in Eq. (39). Plots such as those in Figs. 10 and 12 make it clear that, as in the quartic double-well case, $\mathcal{C}$ can generally be deformed to pass from the initial point q_0 to the final asymptotic position, associated with the singularity, via a sequence of complex turning points so that the real quantity t_* can be decomposed into a sum of complex times associated with passage between these points. Although general systems with barriers may have an unlimited number of complex turning points, the most important of these for the present analysis is the pair, denoted by q_a and q_b, describing collisions with the barrier. These are simply the generalization of the inner turning points $+q_-$ and $-q_-$ for the symmetric double-well systems. For real energies below the barrier maximum ($E<E_s$), these points are located on the real q axis to the right ($q_s-q_a>0$) and left ($q_s-q_b<0$) of the potential maximum. For real energies above the barrier maximum ($E>E_s$), these points are located in the complex plane at

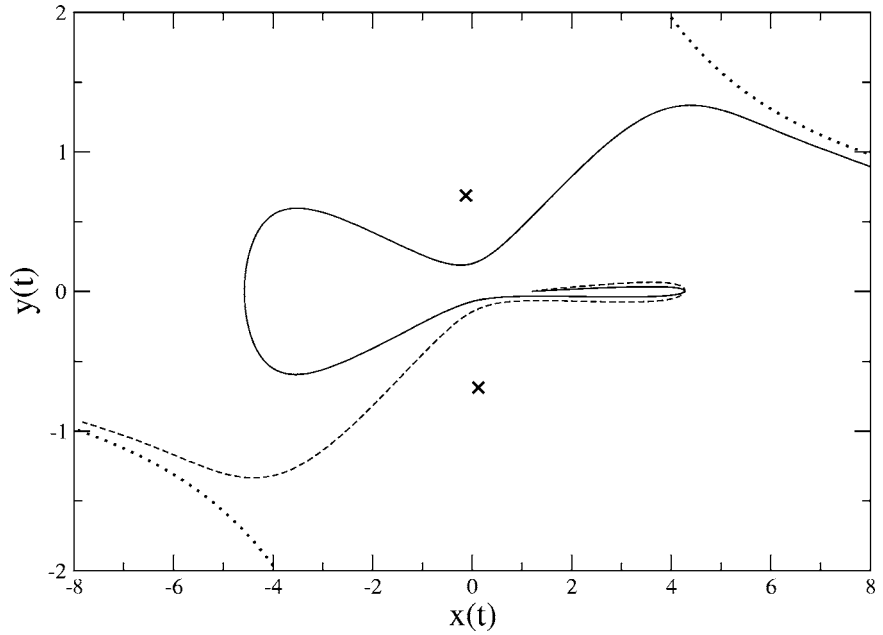

FIG. 12. Singular trajectories corresponding to points on the singularity curves in Fig. 11. The solid curve is obtained for $p_0=(2.6,0.06055)$, corresponding to a point on the lower curve, and the dashed curve is obtained for $p_0=(2.6,0.12038)$, corresponding to a point on the upper curve. The dotted curves show the function $y=\pi/(2\alpha x)$, consistent with Eq. (54) with $k=0$. The $\times$'s mark turning points $\pm q_-$ for the dashed curve. On the scale shown, they are practically identical to the $\pm q_-$ for the solid curve.

positions immediately below $[i(q_s-q_a)<0]$ and above $[i(q_s-q_b)>0]$ the potential maximum, and purely real trajectories pass through the region between them along the real q axis. Examination of plots such as those in Figs. 5, 10, and 12, and similar plots for additional systems (e.g., the Eckart barrier and the pendulum) now leads to the following key observation: similar to real trajectories with $E>E_s$, all singular CD trajectories studied here pass through the region between q_a and q_b [i.e., cross a straight line connecting these points] at least once before becoming singular. As $E\to E_s$, q_a and q_b approach q_s. This constrains a trajectory passing between these points to cross directly through the HFP so that the passage time across the barrier becomes infinite. If such a trajectory is singular, the singularity time tends to infinity.

We now show that a singular CD trajectory, passing at least once through the region between q_a and q_b with $|E-E_s|$ sufficiently small, is indeed part of a continuous family of trajectories that remain singular as $E\to E_s$. In other words, such a trajectory lies on a singularity curve that approaches the separatrix energy as $t_*\to\infty$. To establish this, let us isolate a portion of the curve $\mathcal{C}$ that crosses a straight line connecting q_a and q_b. We deform such a segment of $\mathcal{C}$ to a straight line extending along the real q-axis between points q_1 and q_2, where $q_1>q_s$ and $q_2<q_s$ are real, energy-independent constants with values that need not be precisely specified. Denoting the complex time along this segment by

$$T(E)=\int_{q_1}^{q_2} dq/p(q,E), \tag{55}$$

the singularity time can be expressed in the general form

$$t_*(E)=mT(E)+t_c(E) \tag{56}$$

where $m=1,2,3,\ldots$, is the number of times the deformed trajectory crosses the barrier maximum at $q=q_s$ (i.e., the number of times the original trajectory crosses the line connecting q_a and q_b) and t_c is the complex time for motion along the remaining portions of the deformed trajectory [which exclude the interval (q_2,q_1)]. In Figs. 10 and 12, $m=1$ for the dashed curves and $m=2$ for the solid curves. As before, the condition $\mathrm{Im}\, t_*(E)=0$ identifies energies E of CD singular trajectories and, thus, determines singularity curves.

To proceed, we need to estimate $T(E)$ for energies near E_s. We thus linearize the equations of motion for $q\approx q_s$, replacing the exact Hamiltonian with the approximation $H=p^2/2-\Omega^2(q-q_s)^2/2+E_s$, where $\Omega=[-d^2V(q_s)/dq_s^2]^{1/2}$. If the trajectory begins at point q_1 near q_s with a complex momentum p_1, the complex time required for the system to reach the point q_s is found to be

$$t_{1s}\equiv\int_{q_1}^{q_s}\frac{dq}{p(q,E)}=\frac{1}{\Omega}\tanh^{-1}\left(-\frac{\Omega q_1}{p_1}\right). \tag{57}$$

Expressing p_1 in terms of E and q_1, applying the logarithmic form of the function $\tanh^{-1}(z)$, and expanding to lowest order about $E=E_s$, yields the approximation

$$t_{1s}\approx-(2\Omega)^{-1}\ln[(E-E_s)/E_0], \tag{58}$$

where $E_0=2\Omega^2q_1^2$. Although this result is based on the assumption that $|q_s-q_1|$ is small, so that $V(q_1)$ is approximately quadratic, it can be extended to more general values of q_1 by an appropriate redefinition of the constant E_0. Replacing (q_1,p_1) with (q_2,p_2), we may apply the same treatment to the passage time t_{s2} between q_s and q_2. This yields the approximation

$$T(E)=t_{1s}+t_{s2}\approx-\Omega^{-1}\ln[(E-E_s)/E_0], \tag{59}$$

where E_0 is a certain real constant whose precise value is not important here. The crucial point is that T diverges logarithmically as $E\to E_s$. In contrast, the quantity t_c varies slowly near $E=E_s$ since it describes times for motion along portions of the trajectory that do not pass near the HFP.

We now substitute Eq. (59) into Eq. (56). Treating $t_c=t_{cr}+it_{ci}$ as approximately constant near $E=E_s$, we may solve for E in terms of t_*, to obtain

$$E-E_s=E_0e^{-\Omega(t_*-t_{cr})/m}e^{-i\Omega t_{ci}/m}. \tag{60}$$

This equation provides an explicit formula for the energies of CD singularities as a function of the (real) singularity time t_* and establishes that these energies tend to E_s as $t_*\to\infty$. As in the case of Eq. (26), Eq. (60) implies that the singularity curves in the complex p_0-plane approach the separatrix momentum at specific angles $\theta=-\Omega t_{ci}/m$. We note that the quantities t_{ci} and m appearing here depend on which turning points are encompassed by the singular trajectories and how many times they are encompassed. As in the quartic double well case, the correspondence of specific sequences of turning points to specific singularity curves results in the formation of singularity curve hierarchies for more general double-well systems.

V. SUMMARY AND DISCUSSION

We have examined singularities occurring in classical dynamics for finite real times and complex initial conditions for a number of one-dimensional double-well systems. Our principal objective has been to determine how such singularities influence the ordinary real motion. We began by examining the analytical expressions for the dynamics of the quartic double well system. In that case, we were able to show that the motion becomes singular for a doubly infinite sequence of complex initial conditions, associated with pairs of integers (m,n). These conditions form three-dimensional surfaces in the four-dimensional phase space. For fixed initial coordinate q_0, such surfaces reduce to a dense set of one-dimensional singularity curves in (p_{0x},p_{0y}) space. These curves are parametrized by the singularity time t_* and converge to specific points $p_s^{\pm}$ as $t_*\to\infty$, corresponding to initial momenta for the separatrix. The direction of approach of the curves to $p_s^{\pm}$ depends on (m,n).

Although this confluence of singularities should imply a relationship between the dynamics of complex singular motion and that of the real motion at the separatrix, the nature of this relationship is somewhat subtle. The separatrix motion, which is actually nonsingular for all finite real times, be-

comes singular in the double limit $\lim_{E\to 0}\lim_{t\to t_E}$, where t_E, the time for being in a particular left or right well at energy E, becomes infinite when E approaches the separatrix energy 0. However, the singularity produced, a pole in $\partial q/\partial E$, is of a different kind than the CD singularities and, unlike the CD singularities, is not associated with divergence of the trajectory. Nevertheless, our analysis shows that the two forms of singularities are interrelated: the relatively weak singularity, characteristic of the real separatrix motion, is what remains of the merging CD singularities when their divergent behavior is removed [e.g, by the factor E^m in Eq. (36)]. Thus, although the dynamics at the real separatrix is not identical to the dynamics of singular complex motion, the unstable behavior that characterizes the separatrix can be said to originate from the CD singularities. We mention that it is not difficult to carry out a similar analysis for the singularites of the Eckart system and show that it leads to analogous conclusions.

Several aspects of the analytical results for the quartic oscillator system were verified numerically. Calculations indeed suggest that an infinite number of singularity curves exist and that they approach the initial conditions defining the real separatrix from a variety of directions as t_* becomes large. Each of these singularity curves is found to be associated with trajectories of a particular topology, executing a specific number of cycles in the right and left wells before becoming divergent. This allows one to identify each curve by means of a dynamical code that is shown to be related to the integers (m,n) which identify the singularities in the analytical treatment. The observed ordering of the curves in the complex p_0 plane and their directions of approach to the separatrix can be understood on the basis of the analytical treatment.

The numerical results for this system reveal further apparent relationships between real separatrix dynamics and CD singularities. Like the separatrix, a singularity curve divides phase space into regions of initial conditions that yield qualitatively different long-time dynamics. Additionally, the HFP, responsible for the instability of the real separatrix, also appears to play a critical mechanistic role in the formation of the CD singularities by deflecting trajectories towards divergence channels.

Many of the singularity phenomena described above were also observed in the numerical treatments of two additional double-well systems. In those cases, too, there appeared to be a large number of singularity curves that converge, as $t_*\to\infty$, to the point p_s^+ on the p_0 plane corresponding to the separatrix. These curves also divide the phase space of initial conditions into regions of different dynamics. Although the divergence channels differ greatly for the various systems, entrance into such channels always appears to require a deflection of the trajectory from the HFP.

The apparent generality of the convergence of CD singularities to the separatrix can be traced to a key property of the singular trajectories observed for all systems studied: the passage of these trajectories through the region between a specific pair of complex turning points, associated with barrier collisions. Our analysis establishes that, if a singularity curve associated with such a trajectory passes sufficiently close to the separarratrix, it will actually approach the separatrix as the singularity time becomes infinite. Here, "sufficiently close" means that the turning points for the barrier collisions lie on the portion of the potential energy function that is effectively quadratic. Our treatment directly relies on the existence of the HFP which slows the motion of trajectories in its vicinity, causing the singularity time to diverge, and the singularity energy to approach the real separatrix value.

There is an additional, rather different, argument that ties the delay of the trajectories near the HFP to the approach of CD singularities to the separatrix. It can be proven that, if the potential energy function $V(q)$ is analytic in a strip near the real q axis and has barrier maxima for real q, then the singularity curves (for finite-code singularities) can approach the real axis only at separatrices and only as $t_*\to\infty$. To see this, we note that, for precisely real initial conditions, the trajectory remains real for all t. The analyticity of the potential energy function implies that the dynamics is a continuous function of the initial conditions. Therefore, as the initial conditions approach real values, the trajectory remains nearly real for times approaching infinity [46]. Since singular behavior requires the trajectory to move away from the real q axis, such divergences for initial conditions arbitrarily close to the real axis can arise only as $t_*\to\infty$. Now consider complex initial conditions that tend to real values at energies that do not coincide with those for the separatrix. Since the period of the real motion away from the separatrix is finite, the requirement $t_*\to\infty$ means that such complex initial conditions can produce singularities only if the trajectories survive for an infinite number of periods before diverging, i.e., only if they have codes of infinite length [e.g., r^∞ or $(rl)^\infty$]. It is only for initial conditions near the separatrix, where the period of real motion becomes infinite, that the complex motion can become divergent after a finite number of periods. Thus, initial conditions for CD singularities, associated with finite-length codes, can become real, and the corresponding singularity curves can approach the real axis, only at a separatrix.

As emphasized in Sec. I, complex dynamics is a direct generalization of ordinary, real, classical mechanics and is, thus, a very natural subject for investigation. The present studies were prompted by a surprising lack of previous attention to a conspicuous feature that characterizes these dynamics, namely, the occurrence of singularities and near singularities at finite real times. Since such phenomena occur even in very simple, one-dimensional, autonomous, systems having nonsingular real motion, the present work was restricted to cases of this kind. However, it would be of greater interest to investigate CD singularities in one-dimensional systems that are made nonintegrable by the addition of a time-dependent perturbation. Indeed, as mentioned earlier, there is reason to expect a link, in such systems, between an approach of CD singularities to the real axis and the formation of chaos. We intend to investigate this issue in a subsequent paper which will also demonstrate that many features of the CD singularity behavior found here are shared by such nonintegrable systems. Observed differences in the CD singularity behavior for the two kinds of systems are directly related to specific differences in their real dynamics that arise from their integrable or nonintegrable nature.

ACKNOWLEDGMENTS

This work was supported by the Israel Science Foundation (Grant No. 85/03).

APPENDIX: PROPERTIES OF THE COMPLEX PASSAGE TIMES

We wish to establish the properties described in Sec. II for the variables ρ,σ,μ,ν, and τ_i, defined in Eqs. (16)–(18). Let us denote the quantity $(1+E)^{1/2}$ by z so that $q_\pm^2=1\pm z$ and $k^2=2z/(1+z)$ [see Eqs. (4), (5)]. For the complex momentum range $p_{0x}>0$, $p_{0y}\geq 0$, it is easily verified that $\mathrm{Re}\, z>0$, $\mathrm{Im}\, z\geq 0$, $\mathrm{Re}\, k^2>1$, and $\mathrm{Im}\, k^2\geq 0$. For such values of k^2, a treatment analogous to that of Ref. [42] shows that $K-iK'$ can be expressed in the form

$$K-iK'=\int_0^1 (k^2-u^2)^{-1/2}(1-u^2)^{-1/2}du, \tag{A1}$$

showing that this function becomes real as $\mathrm{Im}\, k\to 0$. Applying this expression, we can write Eq. (16) as

$$\sqrt{2}(\rho-i\sigma)=\int_0^1 (2z-u^2-zu^2)^{-1/2}(1-u^2)^{-1/2}du. \tag{A2}$$

Since, for all $0\leq u\leq 1$, the real part and imaginary parts of $(2z-u^2-zu^2)^{-1/2}$ are >0 and ≤ 0, respectively, it follows that $\rho>0$ and $\sigma\geq 0$.

In a similar way, the representation

$$K'=\int_0^1 (1-u^2+k^2u^2)^{-1/2}(1-u^2)^{-1/2}du \tag{A3}$$

[equivalent to that of Eq. (12)] allows Eq. (17) to be expressed as

$$\sqrt{2}(\mu-i\nu)=\int_0^1 [(1+z)(1-u^2)+2zu^2]^{-1/2}(1-u^2)^{-1/2}du. \tag{A4}$$

Since, for all u in the integration range, the real part and imaginary parts of $[(1+z)(1-u^2)+2zu^2]^{-1/2}$ are >0 and ≤ 0, respectively, we see that $\mu>0$, $\nu\geq 0$.

To establish that $\sigma/\mu\leq 1$, we examine the function

$$q_+^{-1}K=q_+^{-1}\int_0^1 (1-k^2u^2)^{-1/2}(1-u^2)^{-1/2}du \tag{A5}$$

$$=\int_0^1 (1+z-2zu^2)^{1/2}(1-u^2)^{-1/2}du. \tag{A6}$$

Substituting $v=1-2u^2$ for $0<u<2^{-1/2}$ and $v=2u^2-1$ for $2^{-1/2}<u<1$, we obtain

$$q_+^{-1}K=\frac{1}{2}\int_0^1 \frac{1}{(1-v^2)^{1/2}}\left[\frac{1}{(1+zv)^{1/2}}+\frac{1}{(1-zv)^{1/2}}\right]dv. \tag{A7}$$

Denoting $1+zv$ by $r_1\exp(i\phi_1)$ and $1-zv$ by $r_2\exp(i\phi_2)$, we have

$$\mathrm{Im}\left[\frac{1}{(1+zv)^{1/2}}+\frac{1}{(1-zv)^{1/2}}\right]=-r_1^{-1/2}\sin(\phi_1/2)-r_2^{-1/2}\sin(\phi_2/2). \tag{A8}$$

We observe that $r_1>r_2$, and $\pi/4\geq\phi_1/2\geq 0\geq\phi_2/2\geq-\pi/2$. Additionally, since $\sin\phi_1=(\mathrm{Im}\, z)u/r_1$ and $\sin\phi_2=-(\mathrm{Im}\, z)u/r_2$, we have $|\sin\phi_2|>\sin\phi_1$ which, for the above range of ϕ_1 and ϕ_2, implies that $|\sin(\phi_2/2)|>\sin(\phi_1/2)$. As a result, the quantity in Eq. (A8) is positive for all v in the integration range, establishing that

$$\mathrm{Im}\, q_+^{-1}K>0. \tag{A9}$$

Expressing $\mathrm{Im}\, q_+^{-1}K=\mathrm{Im}\,[q_+^{-1}(K-iK')+q_+^{-1}iK']=\sqrt{2}(-\sigma+\mu)$, we see that the above result implies $\mu>\sigma$ or, equivalently, $\sigma/\mu<1$, as claimed.

To examine the asymptotic behavior of σ/μ as $p_{0y}\to\infty$, we note the representations

$$\sqrt{2}(\rho-i\sigma)=\frac{1}{2}\int_0^1 \frac{dw}{[w(1-w^2)(z-w)]^{1/2}} \tag{A10}$$

and

$$\sqrt{2}(\mu-i\nu)=\frac{1}{2}\int_0^1 \frac{dw}{[w(1-w^2)(z+w)]^{1/2}} \tag{A11}$$

which can be obtained by substituting $w=u^2/(2-u^2)$ in Eq. (A2) and $w=(1-u^2)/(1+u^2)$ in Eq. (A4). As $p_{0y}\to\infty$, $z\to 2^{-1/2}\exp(i\pi/2)p_{0y}$ so that $(z\pm w)^{-1/2}\to 2^{1/4}\exp(-i\pi/4)/p_{0y}^{1/2}$. Thus, taking the imaginary part of Eq. (A10) and the real part of Eq. (A11) we find that σ and μ approach the same limiting value

$$2^{-7/4}p_{0y}^{-1/2}\int_0^1 dw[w(1-w^2)]^{-1/2},$$

thus proving that $\sigma/\mu\to 1$ as $p_{0y}\to\infty$.

Finally, we wish to establish bounds for the quantity $\tau_i=\mathrm{Im}\,\tau$ for real values of the initial position q_0. To obtain an upper bound, we express τ (the complex time required for the particle to go from q_0 to the turning point q_+) as

$$\tau=J-T, \tag{A12}$$

where

$$J=\int_{q_0}^\infty dq[2(E-q^4+2q^2)]^{-1/2} \tag{A13}$$

is the time required to travel from q_0 to ∞ and

$$T=\int_{q_+}^\infty dq[2(E-q^4+2q^2)]^{-1/2} \tag{A14}$$

is the time required to travel from q_+ to ∞. The integration paths for J and T can be chosen as straight lines—there are no intermediate singularities that need to be avoided. The substitution $u=q_+/q$ allows us to express T as

$$T = -\frac{i}{\sqrt{2}q_+}\int_0^1 \frac{du}{[1-(q_-/q_+)^2u^2]^{1/2}(1-u^2)^{1/2}} \quad \text{(A15)}$$

$$= -i(2q_+^2)^{-1/2}K' \quad \text{(A16)}$$

$$= -i\mu - \nu, \quad \text{(A17)}$$

where we have used Eqs. (A3) and (17). Taking the imaginary part of both sides of Eq. (A12) now gives $\tau_i = \mathrm{Im}\, J + \mu$. However, since the integration path for J can be chosen to be the real axis, Eq. (A13) shows that $\mathrm{Im}\, J < 0$. Consequently, the equation for τ_i implies that $\tau_i < \mu$, thus establishing the desired upper bound for τ_i.

To obtain a lower bound for τ_i, we express τ in the form

$$\tau = S - I, \quad \text{(A18)}$$

where

$$S = \int_0^{q_+} dq[2(E - q^4 + 2q^2)]^{-1/2} \quad \text{(A19)}$$

and

$$I = \int_0^{q_0} dq[2(E - q^4 + 2q^2)]^{-1/2} \quad \text{(A20)}$$

are times for passage between 0 and q_+ and between 0 and q_0, respectively. Again, we can choose the integration paths in these definitions as straight lines. However, the substitution $u = (1 - q^2/q_+^2)^{1/2}$ converts the integral in Eq. (A19) to the form of Eq. (A1), thus showing S to be identical to $\rho - i\sigma$. As a result, the imaginary part of Eq. (A18) can be expressed as $\tau_i = -\sigma - \mathrm{Im}\, I$. However, since the integration contour for I can be chosen to be the real axis, Eq. (A20) shows that $\mathrm{Im}\, I \leqslant 0$, thus establishing the inequality $\tau_i \geqslant -\sigma$ which provides a lower bound for τ_i.

[1] J. H. Van Vleck, Proc. Natl. Acad. Sci. U.S.A. **14**, 178 (1928).
[2] M. C. Gutzwiller, J. Math. Phys. **8**, 1979 (1967).
[3] W. H. Miller and T. F. George, J. Chem. Phys. **56**, 5668 (1972).
[4] F. Grossmann and E. J. Heller, Chem. Phys. Lett. **241**, 45 (1995).
[5] N. T. Maitra and E. J. Heller, Phys. Rev. Lett. **78**, 3035 (1997).
[6] A. Shudo and K. S. Ikeda, Phys. Rev. Lett. **74**, 682 (1995).
[7] K. G. Kay, J. Chem. Phys. **107**, 2313 (1997).
[8] M. Saltzer and J. Ankerhold, Phys. Rev. A **68**, 042108 (2003).
[9] W. H. Miller, J. Chem. Phys. **95**, 9428 (1991).
[10] M. F. Herman and E. Kluk, Chem. Phys. **91**, 27 (1984).
[11] K. G. Kay, J. Chem. Phys. **100**, 4377 (1994).
[12] Y. Weissman, J. Chem. Phys. **76**, 4067 (1982).
[13] J. R. Klauder, Phys. Rev. Lett. **56**, 897 (1996).
[14] D. Huber and E. J. Heller, J. Chem. Phys. **87**, 5302 (1987).
[15] D. Huber, E. J. Heller, and R. G. Littlejohn, J. Chem. Phys. **89**, 2003 (1988).
[16] S. Adachi, Ann. Phys. (N.Y.) **195**, 45 (1989).
[17] A. L. Xavier and M. A. M. de Aguiar, Ann. Phys. (N.Y.) **252**, 458 (1996).
[18] T. Onishi, A. Shudo, K. S. Ikeda, and K. Takahashi, Phys. Rev. E **64**, 025201(R) (2001).
[19] T. Van Voorhis and E. J. Heller, Phys. Rev. A **66**, 050501(R) (2002).
[20] M. Baranger, M. A. M. de Aguiar, F. Keck, H. J. Korsch, and B. Schellhaaß, J. Phys. A **34**, 7227 (2001).
[21] M. A. M. de Aguiar, M. Baranger, L. Jaubert, F. Parisio, and A. D. Ribeiro, J. Phys. A **38**, 4645 (2005).
[22] T. Shnerb and K. G. Kay, Nonlinear Dyn. **42**, 165 (2005).
[23] O. Brodier, P. Schlagheck, and D. Ullmo, Ann. Phys. (N.Y.) **300**, 88 (2002).
[24] K. Takahashi and K. S. Ikeda, Found. Phys. **31**, 177 (2001).
[25] K. Takahashi, A. Yoshimoto, and K. S. Ikeda, Phys. Lett. A **297**, 370 (2002).
[26] K. Takahashi and K. S. Ikeda, J. Phys. A **36**, 7953 (2003).
[27] C. M. Bender, S. Boettcher, and P. N. Meisinger, J. Math. Phys. **40**, 2201 (1999).
[28] A. Nanayakkara, J. Phys. A **37**, 4321 (2004).
[29] J. D. Doll, T. F. George, and W. H. Miller, J. Chem. Phys. **58**, 1343 (1973).
[30] M. J. Ablowitz, A. Ramani, and H. Segur, J. Math. Phys. **21**, 715 (1980).
[31] Y. F. Chang, M. Tabor, and J. Weiss, J. Math. Phys. **23**, 531 (1982).
[32] J. Fournier, G. Levine, and M. Tabor, J. Phys. A **21**, 33 (1988).
[33] A. Goriely and M. Tabor, Physica D **85**, 93 (1995).
[34] T. Bountis, Physica D **86**, 256 (1995).
[35] A. S. Fokas and T. Bountis, Physica A **228**, 236 (1996).
[36] J. M. Greene and I. C. Percival, Physica D **3**, 530 (1981).
[37] V. I. Arnol'd, Russ. Math. Surveys **18**, No. 5, 9 (1963).
[38] B. V. Chirikov, Phys. Rep. **52**, 265 (1979).
[39] A. J. Lichtenberg and M. A. Lieberman, *Regular and Chaotic Dynamics* (Springer, New York, 1991).
[40] L. Reichl, *The Transition to Chaos In Conservative Classical Systems: Quantum Manifestations* (Springer, New York, 1992).
[41] I. S. Gradshteyn and I. M. Rhyzhik, *Table of Integrals Series and Products* (Academic, New York, 1965).
[42] E. T. Whittaker and G. N. Watson, *A Course of Modern Analysis* (Cambridge University Press, London, 1965); p. 502.
[43] M. Abramowitz and I. A. Stegun, *Handbook of Mathematical Functions* (National Bureau of Standards, Washington, D.C, 1964), Eq. (4.3.93).
[44] A. Goriely and C. Hyde, Phys. Lett. A **250**, 311 (1998).
[45] There are, however special cases in which no such deflections will occur. For example, if the initial position is chosen to coincide with the barrier maximum ($q_0=0$) and the initial momentum p_0 is pure imaginary, the trajectory will diverge directly to $\pm i\infty$.
[46] E. Hille, *Ordinary Differential Equations in the Complex Domain* (Dover, New York, 1976).